

Passivation of CdSe Quantum Dots by Graphene and MoS₂ Monolayer Encapsulation

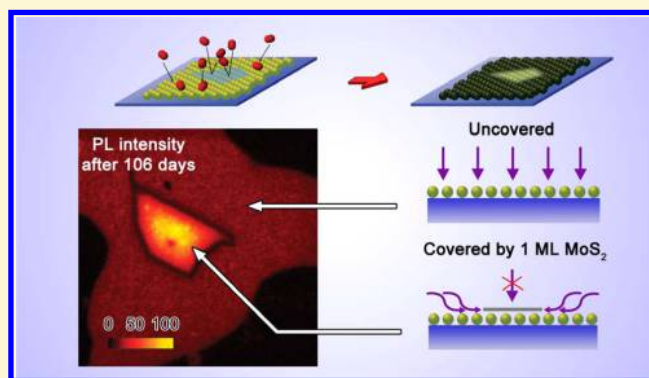
Datong Zhang,[†] Dennis Zi-Ren Wang,[†] Richard Creswell,[†] Chenguang Lu,[‡] Jonathan Liou,[†] and Irving P. Herman^{*†}

[†]Department of Applied Physics and Applied Mathematics, Columbia University, New York, New York 10027, United States

[‡]National Center for Nanoscience and Technology, Beijing 100190, China

Supporting Information

ABSTRACT: The encapsulation of a monolayer of CdSe quantum dots (QDs) by one-to-three layer graphene and MoS₂ sheets protects the QDs from oxidation. Photoluminescence (PL) from the QD cores shows a much slower decrease in core diameter over time due to slower oxidation in regions where the QDs are covered by van der Waals (vdW) layers than in those where they are not, for chips stored both in the dark and in the presence of light. PL mapping shows that the CdSe QDs under the central part of the vdW sheet age slower than those near its edges, because oxidation of the covered QDs is limited by transport of oxygen from the edges of the vdW sheets and not transport across the vdW layers. The transport of oxygen to the covered QDs is analyzed by coupling the PL results and a model of QD core oxidation.



INTRODUCTION

CdSe quantum dots (QDs) with core surfaces capped by ligands are known to deteriorate in air, by oxidation at the surface of the core that can occur in the dark and occur even faster in the presence of light.^{1–6} This leads to a decrease in the diameter of the core, which is accompanied by a decrease in the wavelength of absorption and luminescence and often a decrease in photoluminescence (PL) intensity. This product oxide shell also serves as a barrier to the transport of charge, including electrons, holes, and excitons. To improve and stabilize luminescence efficiency, semiconductor shells are sometimes grown on the cores of CdSe QDs with Type I band alignment, such as ZnS shells.^{7,8} Photoexcitation of these core/shell QDs can still be transferred to nearby materials by Förster resonant energy transfer (FRET),^{9,10} but the movement of electrons and holes and excitons is slowed by this barrier.⁸ When the movement of charges is desired, alternative methods of passivation of the cores are needed that are consistent with the use of the QDs. Using shorter capping ligands or removing ligands could improve charge transfer, but can lead to faster oxidation of the core, which would slow charge transfer.

The prospect of passivating QDs by van der Waals (vdW) materials is raised by the use of chemical vapor deposited graphene to protect metal substrates from oxidation^{11–18} and theoretical studies of the use of MoS₂ and WS₂ monolayers (MLs) for oxidation protection.¹⁹ By fabricating and studying heterostructures of graphene and QD MLs,²⁰ we show that CdSe QD MLs can be passivated well by covering them with van der Waals (vdW) materials, such as graphene and MoS₂,

that are one to several MLs thick. Because vdW MLs absorb light very weakly, this is a potentially interesting way to passivate QDs in a range of optoelectronic applications and is also of interest in heterostructures fabricated using QD MLs and vdW layers.²⁰

EXPERIMENTAL SECTION

QD Preparation and QD Monolayer Preparation. CdSe QDs with a 3.1 nm diameter were synthesized by hot-injection methods (300 °C with cadmium oleate, from CdO, and trioctylphosphine selenide (TOPSe) precursors),²¹ their ligands were exchanged to oleates, and they were stored in a glovebox to minimize exposure to air. Within the glovebox, close-packed QD MLs were then formed by drop-casting 100 μ L of the colloids of QDs in hexane on a \sim 10 cm² dimethyl sulfoxide (DMSO) subphase. After the alkane solvents evaporated, a ML of QDs remained, floating on top of the DMSO,²⁰ which were then scooped up on a chip (Piranha cleaned Si wafers with \sim 300 nm thermally grown oxide) (Figure 1). In one case, the QD ML was scooped onto a chip with a predeposited graphene sheet. (see Figure S4 in the Supporting Information).

Fabrication of the vdW Sheet/QD ML Structure. The QD ML assembly on the chip was then overlaid by several sheets of few-layer graphene or MoS₂, by standard dry transfer methods (Figure 1),²² in an ambient environment, and within 10 min of removal from the glovebox. In this procedure, a separate silicon chip was coated with a layer of polyvinyl alcohol (PVA) and poly(methyl methacrylate) (PMMA) (\sim 280 nm thick) for optimized visual contrast to help

Received: April 24, 2015

Revised: June 18, 2015

Published: June 19, 2015

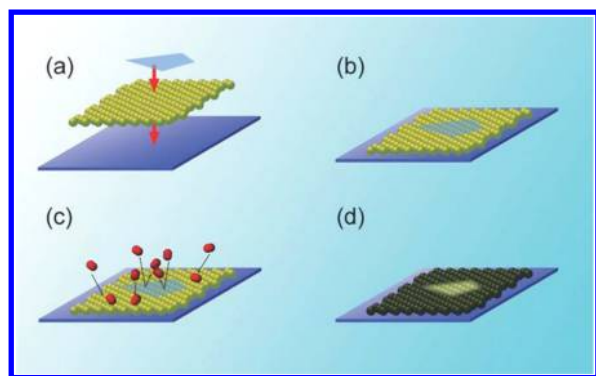


Figure 1. Schematic of the experimental procedures and the effect of vdW monolayer encapsulation. (a, b) A monolayer of CdSe QDs (yellow) is deposited onto the Si chip (with ~ 300 nm thermally grown SiO_2), followed by the dry transfer of few-layer vdW sheets (blue). (c) Oxygen molecules (red) react with the uncovered QDs over time, while the QDs are protected from oxidation in the covered region. (d) QDs near the center of the covered region are observed to age more slowly than those in uncovered regions.

identify the sheet locations and thicknesses. The graphene and MoS_2 vdW sheets were transferred onto these PMMA/PVA/Si chips via mechanical exfoliation by scotch tape (“scratching”). These chips were suspended in water to dissolve the PVA, leaving floating films of PMMA covered with the vdW sheets. Metal scoopers with polydimethylsiloxane (PDMS) covering holes at one end were used to carefully scoop up these films, with the desired vdW sheet(s) clearly visible through the center of the holes. The scoopers were then flipped upside down and positioned with the vdW sheet(s) hovering on top of the QD ML. Contact between the PMMA film and the QDs was made at 30°C , and the temperature increased gradually to 120°C to bring PMMA above its glass transition temperature and detach it from the PDMS. Usually, several sheets were transferred each time, but only one or two were 1, 2, or 3 MLs thick, and these were later examined. The first PL analysis of the chip was then made (0 h). In 4 of the 11 chips, the PMMA overlayer was removed by soaking the chip in acetone for 24 h; this was followed by PL analysis. In these aging experiments, most chips were stored in the dark between PL probing cycles and were in ambient room lighting for ~ 30 min during PL analysis. Each chip was stored individually in a $100\text{ mm} \times 15\text{ mm}$ polystyrene container; the oxygen consumed by the QD MLs during oxidation is negligible compared to that in the container.

The number of MLs in the transferred vdW sheets was determined after scratching by optical microscopy and then confirmed by Raman spectroscopy and also by photoluminescence (PL) for MoS_2 .^{23–25} Using optical microscopy, the shapes of the vdW sheets were approximated as rectangles with shorter and longer side lengths, for classification and analysis. (See the Supporting Information.)

Except as indicated otherwise, the assembly and subsequent analysis of the chips were performed at room temperature.

Optical Excitation and Photoluminescence Collection and Analysis. In point-to-point measurements (Figures 2 and 3), PL was excited using a cw laser at 532 nm with $30\ \mu\text{W}$ power, which was focused to a $\sim 1\ \mu\text{m}$ spot size and measured at several points, as described above. CdSe QD PL was measured from 531 to 587 nm (which does not include the spectral region of PL from a MoS_2 ML) with the spectral region at and near the laser wavelength blocked by an edge filter, with a 1 s integration time (Renishaw system). Each PL spectrum was fit by the sum of a Gaussian and Lorentzian of equal peak wavelength and height, and equal half-width at half-height, to obtain the peak wavelength and intensity, as used in Figures 2 and 3. The spectra were better fit by these profiles than by pure Gaussian or Lorentzian lineshapes. The fit parameters were not sensitive to the details of the fitting methods.

In the other set of experiments, PL was mapped across several structures by scanning a 440 nm ultrafast laser with a 100 ps pulse

width and 10 MHz repetition rate and low-average power ($5\ \mu\text{W}$), at the Center for Functional Nanomaterials (CFN) at the Brookhaven National Laboratory (BNL). The laser was imaged to a $\sim 1\ \mu\text{m}$ spot size on the structure with an optical microscope, and then scanned over the structure ($\sim 0.3\ \mu\text{m}^2/\text{s}$). The PL was measured using a bandpass filter, which peaked at 550 nm and had a full width of 88 nm, to transmit the CdSe QD PL and block the MoS_2 PL (see Figure S1, Supporting Information), using a PicoQuant time-correlated single photon counting (TCSPC) system.

RESULTS

In one set of experiments with chip preparation as portrayed in Figure 1 (and see Figure 6, below), the PL of the closed-packed 3.1 nm diameter CdSe QD ML was measured six times (cycles) over 27 days after the chips were fabricated, the first time within 2 h of vdW transfer. The 11 chips where the QD MLs were also partially covered by vdW sheets (five covered by 1–3 sheets of graphene and six by 1–2 sheets of MoS_2) were probed in regions covered and uncovered by the vdW sheets; reference chips of QD MLs without vdW sheets were also probed. During each measurement cycle, PL was induced by a focused 532 nm cw laser fixed at one of five different random sampling points near the center of each of the vdW sheets atop the QD ML and in the uncovered QD ML regions. In these point-to-point studies, different spots were illuminated in each cycle to avoid interrogating previously illuminated regions where photooxidation could occur (see below). A Raman spectrum of Si was taken three times with the same laser parameters at the beginning, middle, and end of the measurement cycle, and this showed that the collected PL was stable within $\pm 10\%$ during each experiment. After the first PL measurement, right after fabrication, the 225 ± 15 nm thick PMMA backing that initially overlaid the vdW sheets and the otherwise uncovered QD ML on all chips was removed in 4 of the 11 chips by soaking them in acetone for ~ 24 h. Most chips were stored in a dark ventilated box between PL measurement cycles, except for two chips (one with graphene and one with MoS_2 sheets) that were stored under continuous room lighting in a fume hood to examine the effect of light degradation with vdW layer encapsulation.

Figure 2a,b shows representative PL spectra from QDs covered by 1 ML graphene and 1 ML MoS_2 , as well as from uncovered QDs on the corresponding chips. The first set of measurements was taken immediately after chip fabrication and PMMA removal and the last set 27 days later, with chip storage in the dark. The PL is from the CdSe QDs; PL can also be seen from the MoS_2 MLs, but at wavelengths longer than those shown (see Figure S1 in the Supporting Information). There is a substantial decrease in both the intensity and the peak wavelength of the uncovered QDs over this period. There are smaller decreases in the PL peak wavelength in the chip regions covered by a graphene or MoS_2 ML sheet, and little change in PL intensity.

Panels (c) and (d) in Figure 2 plot the mean value and standard deviation of the peak PL wavelengths from the random spots picked near the center of the same chip region during each run. They also show the diameter of the core, d , as determined from the peak wavelength, by using the calibration between the core diameter and first exciton peak in absorption²⁶ and the ~ 70 meV Stokes shift between this absorption peak and the PL peak.²⁷ Aside from the points at 185 h (see below), the diameter of the CdSe core decreases monotonically with time due to oxidation, and this decrease is slower in both covered chip regions than in their uncovered

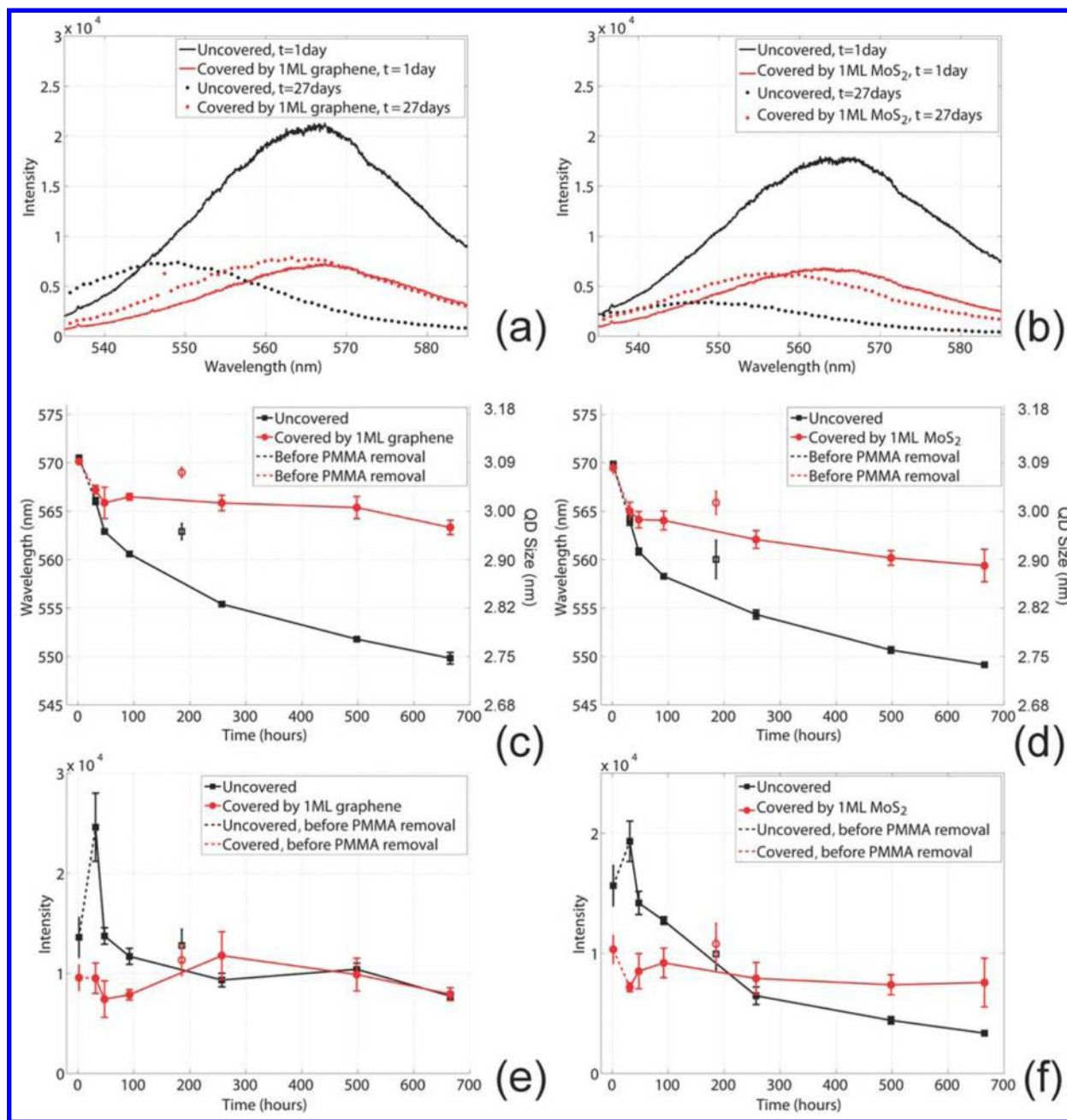


Figure 2. PL of the QD ML that was covered (red) by 1 ML graphene in (a), (c), and (e) and 1 ML MoS₂ in (b), (d), and (f), and uncovered (black) (a–f), excited by a cw 532 nm laser with 30 μ W power. (a, b) PL spectra at the beginning (24 h) (solid lines) and end (27 days) (dashed lines). (c, d) PL peak wavelength vs time, with the QD diameter axis added on the right. (e, f) PL peak intensity vs time. In (c)–(f), the points at 0 h were taken before PMMA overlayer removal, and those at 24 h and later were taken after PMMA removal. Lines connecting the data points (except those at 185 h; see the text) are added to aid viewing.

counterparts due to slower oxidation. Panels (e) and (f) in Figure 2 are the corresponding PL intensities. PMMA still overlaid the chip for the first data point and was removed before subsequent ones were obtained. After PMMA removal, the intensities of uncovered chip regions drop monotonically over the course of the experiment (aside from the points at 185 h), whereas the intensities of the QD PL in covered chip regions fluctuate more or less around their values right after PMMA removal. The data in Figure 2a,c,e are all for the same chip region, as are the data in Figure 2b,d,f. (The Raman intensity count rate from a bare silicon chip was abnormally low, by a factor of 3, during the fifth set of measurements (at

185 h), which was attributed to poor instrument alignment. To try to account for this, the PL integration times were 3 \times longer at 185 h than otherwise. These points, displayed in Figure 2c–f as open symbols, are not included in the lines connecting the points that have been added to aid viewing. The data points in this measurement cycle do not follow the trends that are seen to be very consistent for all other cycles.)

The change in QD core diameter over the 27 day period is plotted for each region probed on each chip in Figure S2 (in the Supporting Information) as a function of the smallest full dimension of the vdW (based on approximating the shape of the vdW sheets as rectangles) and in Figure 3 as a function of

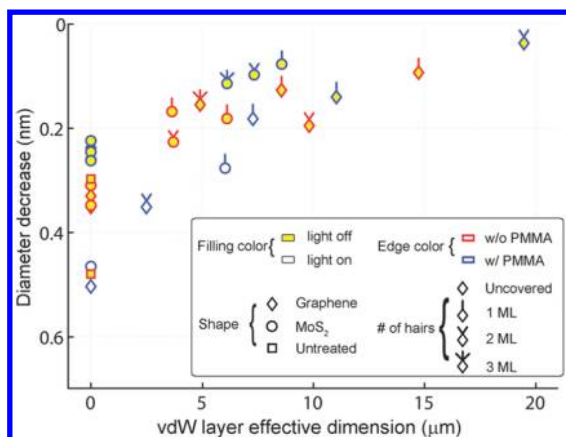


Figure 3. Decrease in QD size (27 days after fabrication) vs the effective dimension of the vdW sheet, with different variables indicated by the appearance of the data points, including the presence of room light illumination (filling color), the presence of a PMMA overlayer (edge color), the type of vdW sheet (shape), and the number of layers in the vdW sheet (number of hairs).

the effective dimension of the vdW sheets. (As detailed in the Supporting Information, this dimension for a vdW sheet (approximated as a rectangle) is defined as the side length of a square for which diffusion from the edges to the center occurs over the same amount of time as the rectangle. Therefore, a $9 \mu\text{m} \times 9 \mu\text{m}$ sheet has an effective dimension of $9 \mu\text{m}$ and a $9 \mu\text{m} \times 23 \mu\text{m}$ sheet has an effective dimension of $\sim 11 \mu\text{m}$.) The dependence on size is very similar in the two plots. The symbols denote the type of vdW material and the number of vdW monolayers (1, 2, or 3), whether the PMMA overlayer was present, and whether the chips were stored in the dark or in the presence of light. All the points at dimension 0 are for the QD MLs not covered by a vdW sheet (sometimes with a PMMA overlayer). Some of these are for regions on chips that have vdW sheets elsewhere (and are consequently subject to the same process procedures as the vdW sheet regions), and others are for reference chips with no vdW sheets.

PL was also measured on several chips by using a 440 nm ultrafast laser (at the Brookhaven National Laboratory) with low-average power imaged on the structure with an optical microscope, and then scanned over the structure ($\sim 1 \mu\text{m}$ spot size). The bandpass filter used transmitted the CdSe QD PL (peak at $\sim 570 \text{ nm}$) and removed the MoS₂ PL (see Figure S1, Supporting Information). No photoinduced changes in the QDs were observed even after multiple scans over the same area with this mapping system, which enabled aging studies; photoinduced changes were seen when scans were made using the 532 nm cw laser, during which $>1000\times$ as many photons impinged on the QDs than with the ultrafast laser, so that system was used only for the above point-to-point study. Figure 4b,c plots emission in the spectral region of CdSe QD PL, for a chip where 1 and 2 ML sheets of MoS₂ overlay regions with (upper right) and without (lower right) a QD ML (Figure 4a) (both with the PMMA overlayer); PL was mapped 24 h and 50 days after chip fabrication. As expected, there is very little signal from regions where there are no QDs, including from the regions where there is only MoS₂. At 24 h, the QD PL is weaker in regions covered by MoS₂ than in those in uncovered regions; these PL variations track the regions shown in the optical micrograph in Figure 4a. At 50 days, the covered areas are brighter than the uncovered areas, but some of the covered

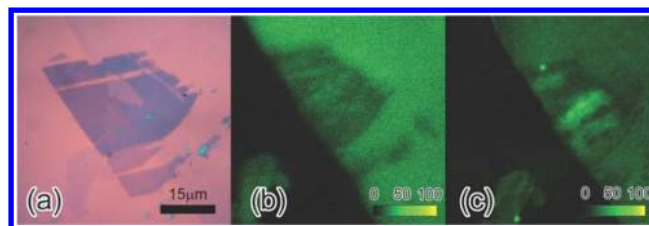


Figure 4. (a) Optical image of 1 and 2 ML MoS₂ sheets transferred onto the edge of a 3.1 nm CdSe QD ML. (b) Map of PL from the CdSe QDs taken 24 h after chip fabrication (with the PMMA overlayer), excited by a scanning 440 nm ultrafast laser. The brighter, green areas indicate PL from the uncovered QD ML, and the dimmer, gray areas indicate PL where the QD ML was covered by few-layer MoS₂. There are no QDs in the dark triangle on the left. (c) PL mapping 50 days after fabrication, showing that the PL from CdSe QDs near the center of the overlaying few-layer MoS₂ was stronger than that from uncovered QDs. The absolute scales are different in (b) and (c).

regions are brighter than others. (PL mapping of an aged structure with the CdSe QD ML overlaying graphene in some regions and overlaid by graphene in others is shown in Figure S4 in the Supporting Information.)

Figure 5 shows the QD emission with a 1 ML MoS₂ sheet in the middle of a QD ML (and not overlapping regions without

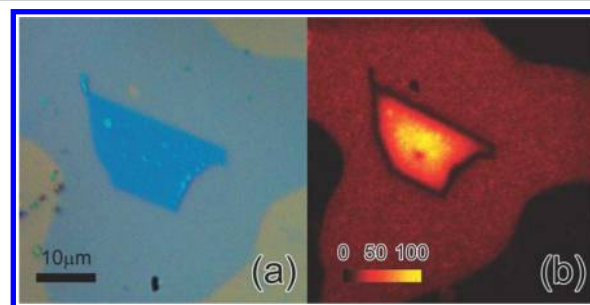


Figure 5. (a) Optical image and (b) PL map of 1 ML MoS₂ sheet transferred onto 3.1 nm CdSe QD ML on a SiO₂/Si chip, taken 106 days after the chip fabrication (with the PMMA overlayer removed). QDs are present in the large light blue area in the background of (a), while the central shape is the 1 ML MoS₂ sheet.

QDs, as in Figure 4), taken 106 days after chip fabrication (with the PMMA removed), along with an optical image of this structure. The QD PL in the covered region is generally brighter than that in the uncovered region and is brighter nearer the center of the covered region than in the outer regions. The QD PL at the edge of the sheet is weaker, even weaker than in QD regions that are totally uncovered by the MoS₂ sheet.

DISCUSSION

General Observations. Overlaying vdW sheets provides good, but not perfect, encapsulation of the QDs. The results in Figures 2–5 are consistent with vdW MLs being very good barriers against O₂ penetration and present a consistent picture when comparing covered and uncovered regions. It is also consistent with the current understanding that semiconductor QD cores oxidize to form smaller cores, surrounded by oxide shells. It is thought that SeO₂ forms on the surface of CdSe QDs in the presence of oxygen in the dark^{1–4} and oxidizes even faster in the presence of light;^{5,6} this has been attributed to the

binding of the surface ligand TOPO to cadmium but not selenium. There is apparently no evidence of cadmium oxidizing in TOPO-covered QDs exposed to air,^{1–3} but there is when it is capped by pyridine.^{2,3} Katari et al.³ found that the oxidized selenium subsequently desorbs.

Therefore, during QD aging, oxygen produces an oxide shell of SeO₂ and perhaps CdO surrounding the shrinking CdSe core. In the early stages of aging, the local O₂ becomes depleted, while the local N₂ remains undepleted, and new oxygen needs to arrive at the outer shell to continue oxidation. In the air trapped by the vdW overlayer, there are an estimated ~ 0.25 O₂ molecules per QD; this produces an ~ 0.0010 nm thick oxide shell (for the moment assuming a continuum model), which is much thinner than a full monolayer of oxide, and decreases the core diameter by only ~ 0.00093 nm. Consequently, assembling the structure in an environment free of O₂ would have little effect on the total QD oxidation here. This trapped air needs to be replaced ~ 290 times to enable oxidation that decreases the diameters of CdSe QD cores from 3.1 to ~ 2.8 nm (as in Figure 3), which requires ~ 75 O₂ molecules per QD (assuming that only the Se is oxidized³). This corresponds to an effective air layer that is at least $1.7 \mu\text{m}$ thick.

Immediately after assembly, the QD PL peaks at the same wavelength, ~ 570 nm, in both the uncovered and covered regions, and blue shifts with time due to oxidation; the shift is much slower in regions covered by vdW layers, which indicates much slower QD oxidation there (Figure 2a–d). More generally, Figure 3 shows that the oxidation of CdSe QDs, as monitored by the decrease in the diameter of the core, (1) decreases when the QDs are blanketed by ~ 225 nm thick PMMA, (2) decreases much more so when overlaid instead by a vdW sheet (which is much thinner than the PMMA layer), and (3) decreases even a bit more when that sheet is blanketed by PMMA (Figure 3). Graphene and MoS₂ sheets slow down oxidation roughly equally. Oxidation is slower for larger vdW sheets (Figure 3). It is not clear (from Figures 3, S2, and S3, Supporting Information) whether oxidation is slower with several-layer vdW sheets than for a single ML, in part because the lateral size of the sheets seems to dominate the trends in this chip set. (Note that the thicker sheets tended to be smaller here.) The 2D transport of O₂ between the vdW sheet and the QD ML from the edges of the sheets to its center appears to be the main route of replenishing O₂ near the QDs (on the basis of Figures 3 and 5), and not transport across the vdW sheet (with or without the PMMA overlayer), as portrayed in Figure 6. The progress of oxidation would likely be even slower than that observed here for even larger vdW sheets; however, it is not clear that there would be no evidence of oxidation. Given previous studies of photodegradation,^{5,6} it is not surprising that oxidation is seen to be faster with storage in the presence of light.

The time variation of the PL intensity (Figure 2e,f) depends on the rate of photoexcitation and the quantum yield [$\gamma_{\text{rad}}/(\gamma_{\text{rad}} + \gamma_{\text{nonrad}})$ for radiative decay rate γ_{rad} and nonradiative decay rate γ_{nonrad}], which, in turn, depend on oxidation and other factors. In the uncovered regions, the PL intensity increased after the PMMA overlayer was removed and then monotonically decreased with time, while its peak blue-shifted monotonically (Figure 2). As the core diameter d decreases, absorption in this optically thin QD ML changes little (Figure S5, Supporting Information). The decrease in the QD absorption cross section at the first exciton peak, which is proportional to $d^{2,6,26}$ is

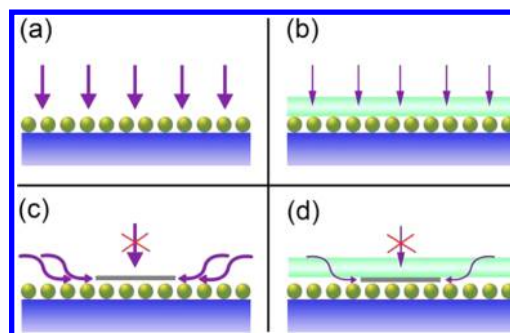


Figure 6. Diagrams of the four types of probed regions on the chips, each with a different assembly of the QD ML with vdW ML or few-layer sheets and PMMA overlayers, with the primary pathways of O₂ flow to the center of the region indicated.

balanced by the increase due to more resonant excitation as the first exciton peak (553 nm for 3.1 nm; 537 nm for 2.8 nm) approaches the 532 nm laser wavelength, so the decay of the PL intensity indicates that the quantum yield of the CdSe QD ML decreases during oxidation. As d decreases, the quantum yield of (uncovered, individual) CdSe QDs is thought to increase, with γ_{rad} increasing and γ_{nonrad} decreasing,²⁸ so the decrease in PL intensity with time for uncovered QDs is likely largely due to the increased nonradiative decay rate at the core/oxide shell interface due to the formation of traps and other defects. The initial increase following PMMA removal may be caused by decreased QD quenching due to FRET from the QDs to the PMMA. Given that graphene absorbs less light than MoS₂, the greater quenching of QD PL right after PMMA removal for QDs covered by graphene may indicate that the QDs are more strongly coupled by FRET to graphene than to MoS₂ for these conditions (and specific distances between the QDs and vdW layer).

The PL from QDs covered by the vdW sheets is weaker than that from uncovered QDs early during the aging run because of the weak absorption in the vdW sheet (for graphene and MoS₂: $\sim 2.3\%$ and $\sim 7.5\%$ per layer at 532 nm and $\sim 2.3\%$ and $\sim 13\%$ at 440 nm^{29,30}), the altered reflection coefficient, and increased nonradiative decay due to FRET to the vdW layer.^{9,10} The subsequent slower decay, and occasional slight increase, of PL intensity suggests that this slower oxidation leads to fewer recombination sites at the core/oxide shell interface.

The slower decay of QD PL intensity with vdW sheets overlaying the QDs is also indicated in the PL maps in Figures 4 and 5. Figure 4 shows that not all of the covered areas were well-protected from oxidation. This is probably because the MoS₂ sheet was placed on the edge of the QD ML, where the ~ 3.1 nm difference in the height of the sheet (due to the size of the QDs) may create an air gap that allows oxygen to diffuse underneath the MoS₂ sheet and diminish encapsulation in some nominally covered regions. There is no corresponding edge region in the geometry for Figure 5, and this effect is not seen. In Figure 5b, the decrease of the QD PL intensity away from the center suggests there is increased oxygen concentration beneath the MoS₂ sheet and nearer to its edges due to 2D diffusion there. This figure also shows very weak QD PL at the very edge of the sheet, which is even weaker than that from QDs in totally uncovered regions. This was also observed in other scans. Nonradiative losses are largest in this region because the QDs are exposed to ambient air and oxidize rapidly (so have the high nonradiative decay rates of QDs in totally

uncovered regions, due to decay routes other than FRET) and are close to the vdW sheets (so there is significant FRET to the vdW sheet, as occurs in the totally covered regions). The lower PL intensity at the MoS₂ edges may also be due to catalytic activity there that degrades the QDs.

Modeling the QD Oxidation. The first part step in oxidation is transport of oxygen from the ambient to the “bulk” near the QD surface. For covered QDs, this would be described by the diffusion equation (for this atomistic limit) in 1D for only a PMMA overlayer and in 2D for diffusion (or permeation) between the vdW sheet overlayer and QD ML-covered substrate. This presumes that there is no significant transport across the vdW sheet, which is supported by the experimental results. (Thermal emission and quantum tunneling transport of O₂ across a vdW ML, with an estimated barrier height of 5 eV and thickness of 0.5 nm from ref 19, provides $\sim 10^{-68}$ \times the flow needed to produce the observed ~ 0.3 nm thick oxide shells over 27 days.) The primary modes of O₂ transport to the QD surface for the different experiments are depicted in Figure 6. This transport is described further below.

The Deal–Grove model of the thermal oxidation of silicon^{31,32} can be applied to QD oxidation, with oxygen: (a) transport from the bulk to the ligand-free QD core surface; (b) diffusion through the oxidized shell to the surface of the remaining QD core; and (c) reaction with the surface of the remaining QD core. The importance of diffusion through the ligand shell will be addressed later. It is reasonable to assume that no gas-phase products are produced directly from step (c) on the basis of models of CdSe oxidation.³ It is also assumed at first that the oxide shell does not desorb during aging (see below). (Transport of direct oxidation products or molecules slowly desorbing from the oxide shell could slow step (a) and tend to decrease the oxidation rate in covered regions. Oxide shell desorption would enhance step (b) because the oxide shell would be thinner, and this would tend to increase the oxidation rate, other things being equal.)

As for Si oxidation, in the oxidation of uncovered QDs, the effective O₂ flux at each step, for a given local “bulk” pressure of oxygen in the gas outside the QDs, C_g , is

$$J_{\text{gas}} = h_g(C^* - C_s) \quad (1)$$

$$J_{\text{oxide}} = -D_{\text{ox}} \nabla C \quad (2)$$

$$J_{\text{react}} = k_i C_i \quad (3)$$

where J_{gas} , J_{oxide} , and J_{react} are the fluxes for the three respective steps, with C_s the oxygen concentration at the outer surface of the oxide and C_i that inside the oxidized shell just outside the remaining core. C^* is the equilibrium value of C_s and is proportional to C_g according to Henry's law. h_g is the gas-phase transport coefficient, D_{ox} is the effective diffusion coefficient of oxygen in the QD oxide shell, and k_i is the reaction rate constant. In steady state, the gas fluxes $4\pi R^2 J$ are the same at each interface, where R is the radius of that shell. Solving eqs 1–3 in spherical coordinates gives the thickness of the oxidized shell with time.³² This assumes that the reaction at the core does not produce volatile products and the oxide layer does not desorb.

The solution to eqs 1–3 is used to compare the oxide thickness as a function of C_g for different measurement conditions. This solution shows that the time t_{ox} required to reach a given oxide layer thickness is proportional to $1/C_g$. This

means that, if these equations were strictly applied to all uncovered and covered regions, decreasing C_g by a factor of x , say, by covering the QD film with a vdW ML, would be equivalent to slowing down other characteristic oxidation times by x . The shape of a curve plotting QD size versus time (from the runs shown in Figures 2 and 3) would then be almost the same for different covered and uncovered chip regions, with the time axis scaling by x (using the scaling procedure described in the Supporting Information). With the O₂ partial pressure near the QDs for uncovered chip regions of ~ 160 Torr for atmospheric conditions, the effective pressure near the QDs for covered chip regions would be ~ 160 Torr/ x . The O₂ in this local bulk environment would be supplied by 2D transport from the ambient near the chip, to the region under the vdW layer, and to the QDs in the center of the chip region (Supporting Information). (Some O₂ may react before reaching the center; if so, the slower oxidation in the center could be explained by this, the transport profile in the absence of QD oxidation, and by how transport could be different through a ML of nonoxidized and oxidized QDs.)

This scaling procedure is found to be approximately valid when comparing the oxidation of QDs that are uncovered and covered on the same chip for chips stored in the dark, as is seen Figure 7 for an overlaying sheet of 1 ML MoS₂ and in Figure

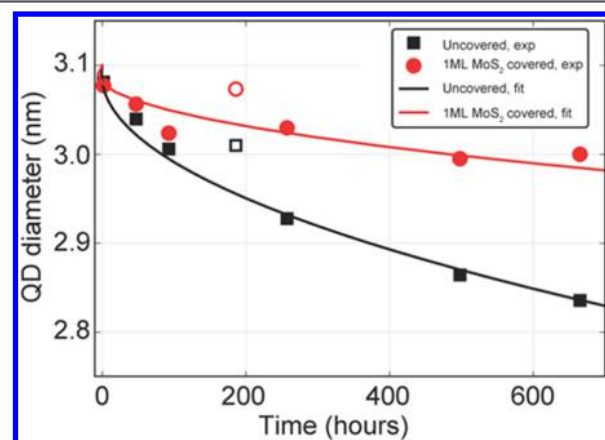


Figure 7. Scaling fit of QD core diameter vs aging duration for regions on a chip where the QD ML is covered by a $7.0 \mu\text{m} \times 53 \mu\text{m}$ MoS₂ ML (with an effective dimension of $8.6 \mu\text{m}$) or uncovered (both with the PMMA overlayer and storage in the dark). The scaling factor is 5.3.

S6a in the Supporting Information for an overlaying sheet of graphene. In each case, the two curves are fit well with the same parabolic function, but with different scaling. The respective scaling factors are ~ 5.3 and 2.1 , which means that, according to this model, the effective O₂ pressure due to the encapsulation is estimated to be ~ 30 and 76 Torr, respectively. The scaling factor increases with sheet dimension (Figure S7 in the Supporting Information). This analysis suggests that the effective diffusion coefficient for 2D transport of O₂ between the vdW layer and the QD ML-covered substrate is $\sim 10^{-10}$ cm²/s, when assuming a 1 nm thick medium. This is smaller than the diffusion coefficient for O₂ in polystyrene³³ of 3.8×10^{-8} cm²/s and larger than that for O₂ in solids such as vitreous SiO₂ (from ref 34, after scaling from the elevated measurement temperature to room temperature) and suggests that the vdW sheet follows the QD ML topography very well, with few gaps, and that this transport is limited by the 2D diffusion across the ligand shells in the QD ML.

This scaling argument could be invalid because it neglects the QD ligand shell. In addition to eqs 1–3, there should be an equation describing the diffusion of oxygen from the “bulk”, through the fixed ligand shell, to the outside of the outer surface of the QD oxide shell. The Supporting Information shows that this scaling procedure is still valid when this fourth equation is included. Scaling would also be rendered invalid if the impact of oxide desorption were different for covered and uncovered chip regions. (The impact of oxide desorption would be stronger in uncovered regions, where it would lead to thinner oxide shells and relatively faster diffusion of O₂ through the oxide shell.) Scaling was found to be less successful when comparing PL from QDs on different chips and QDs on the same chip when the chips were stored in the presence of light (Figure S7, Supporting Information), which is not surprising given the variability in process conditions between different runs and with different storage conditions.

CONCLUSIONS

The encapsulation of a monolayer of CdSe quantum dots by one-to-three layer graphene and MoS₂ sheets protects them from oxidization. Photoluminescence from the QD cores shows a much slower decrease in core diameter, due to slower oxidation, in regions covered by vdW layers than in those where they are uncovered, whether the chips were stored in the dark or in the presence of light. PL mapping shows that the CdSe QDs under the central part of the vdW sheet age slower than those at the edge, because the oxidation of these covered QDs is limited by the transport of oxygen from the edges of the vdW sheets and not oxygen transport across the vdW layers. The partial pressure of oxygen near the covered QDs is determined by coupling the PL results and models of the transport of oxygen and QD oxidation. The overlaying vdW sheets provide good, but not perfect, encapsulation of the QDs, likely due to the limited lateral dimensions of the vdW sheets. We expect the diffusion time scales will be on the order of years for vdW lateral dimensions exceeding ~500 μm, so vdW layer encapsulation would improve prospects for the applications of QD MLs.

ASSOCIATED CONTENT

Supporting Information

Additional information with respect to photoluminescence from a CdSe QD ML/MoS₂ ML structure, determination of the effective dimension of a vdW sheet, additional results of the point-by-point PL studies, photoluminescence from an aged graphene ML/CdSe QD ML/graphene ML structure, QD optical absorption strength, and scaling photoluminescence during chip aging. The Supporting Information is available free of charge on the ACS Publications website at DOI: 10.1021/acs.chemmater.5b01522.

AUTHOR INFORMATION

Corresponding Author

*E-mail: iph1@columbia.edu.

Notes

The authors declare no competing financial interest.

ACKNOWLEDGMENTS

We thank Jiayang Hu for assistance with collecting PL spectra. Support was provided by the MIRT program of the National Science Foundation (DMR-1122594), the NSF MRSEC

program through Columbia in the Center for Precision Assembly of Superstratic and Superatomic Solids (DMR-1420634), the NSF IGERT program (DGE-1069240), the EFRC program of DoE (DE-SC0001085), the New York State Office of Science, Technology, and Academic Research, and a gift by the Honda Research Institute. We thank Drs. Matthew Sfeir and Mircea Cotlet for their assistance in using the ultrafast PL system at the CFN in BNL. This research used resources of the Center for Functional Nanomaterials, which is a U.S. DOE Office of Science Facility, at Brookhaven National Laboratory under Contract No. DE-SC0012704.

REFERENCES

- (1) Maenosono, S.; Ozaki, E.; Yoshie, K.; Yamaguchi, Y. Nonlinear Photoluminescence Behavior in Closely Packed CdSe Nanocrystal Thin Films. *Jpn. J. Appl. Phys.* **2001**, *40*, L638.
- (2) Hay, K. X.; Waisundara, V. Y.; Zong, Y.; Han, M. Y.; Huang, D. CdSe Nanocrystals as Hydroperoxide Scavengers: A New Approach to Highly Sensitive Quantification of Lipid Hydroperoxides. *Small* **2007**, *3*, 290–293.
- (3) Katari, J. B.; Colvin, V. L.; Alivisatos, A. P. X-ray Photoelectron Spectroscopy of CdSe Nanocrystals with Applications to Studies of the Nanocrystal Surface. *J. Phys. Chem.* **1994**, *98*, 4109–4117.
- (4) Li, R.; Lee, J.; Yang, B.; Horspool, D. N.; Aindow, M.; Papadimitrakopoulos, F. Amine-Assisted Faceted Etching of CdSe Nanocrystals. *J. Am. Chem. Soc.* **2005**, *127*, 2524–2532.
- (5) Hines, D. A.; Becker, M. A.; Kamat, P. V. Photoinduced Surface Oxidation and Its Effect on the Exciton Dynamics of CdSe Quantum Dots. *J. Phys. Chem. C* **2012**, *116*, 13452–13457.
- (6) Hines, D. A.; Kamat, P. V. Recent Advances in Quantum Dot Surface Chemistry. *ACS Appl. Mater. Interfaces* **2014**, *6*, 3041–3057.
- (7) Talapin, D. V.; Rogach, A. L.; Kornowski, A.; Haase, M.; Weller, H. Highly Luminescent Monodisperse CdSe and CdSe/ZnS Nanocrystals Synthesized in a Hexadecylamine–Triethylphosphine Oxide–Triethylphosphine Mixture. *Nano Lett.* **2001**, *1*, 207–211.
- (8) Dabbousi, B. O.; Rodriguez-Viejo, J.; Mikulec, F. V.; Heine, J. R.; Mattoussi, H.; Ober, R.; Jensen, K. F.; Bawendi, M. G. (CdSe) ZnS Core–Shell Quantum Dots: Synthesis and Characterization of a Size Series of Highly Luminescent Nanocrystallites. *J. Phys. Chem. B* **1997**, *101*, 9463–9475.
- (9) Chen, Z.; Berciaud, S.; Nuckolls, C.; Heinz, T. F.; Brus, L. E. Energy Transfer from Individual Semiconductor Nanocrystals to Graphene. *ACS Nano* **2010**, *4*, 2964–2968.
- (10) Prins, F.; Goodman, A. J.; Tisdale, W. A. Reduced Dielectric Screening and Enhanced Energy Transfer in Single- and Few-Layer MoS₂. *Nano Lett.* **2014**, *14*, 6087–6091.
- (11) Dedkov, Y. S.; Fonin, M.; Rüdiger, U.; Laubschat, C. Graphene-Protected Iron Layer on Ni (111). *Appl. Phys. Lett.* **2008**, *93*, 022509.
- (12) Dedkov, Y. S.; Fonin, M.; Laubschat, C. A Possible Source of Spin-Polarized Electrons: The Inert Graphene/Ni (111) System. *Appl. Phys. Lett.* **2008**, *92*, 052506.
- (13) Borca, B.; Barja, S.; Garnica, M.; Minniti, M.; Politano, A.; Rodriguez-García, J. M.; Hinarejos, J. J.; Farias, D.; de Parga, A. L. V.; Miranda, R. Electronic and Geometric Corrugation of Periodically Rippled, Self-nanostructured Graphene Epitaxially Grown on Ru (0001). *New J. Phys.* **2010**, *12*, 093018.
- (14) Chen, S.; Brown, L.; Levendorf, M.; Cai, W.; Ju, S. Y.; Edgeworth, J.; Li, X.; Magnuson, C. W.; Velamakanni, A.; et al. Oxidation Resistance of Graphene-coated Cu and Cu/Ni Alloy. *ACS Nano* **2011**, *5*, 1321–1327.
- (15) Gadipelli, S.; Calizo, I.; Ford, J.; Cheng, G.; Walker, A. R. H.; Yildirim, T. A Highly Practical Route for Large-Area, Single Layer Graphene from Liquid Carbon Sources such as Benzene and Methanol. *J. Mater. Chem.* **2011**, *21*, 16057–16065.
- (16) Cho, J.; Gao, L.; Tian, J.; Cao, H.; Wu, W.; Yu, Q.; Yitamben, E. N.; Fisher, B.; Guest, J. R.; Chen, Y. P.; et al. Atomic-Scale Investigation of Graphene Grown on Cu Foil and the Effects of Thermal Annealing. *ACS Nano* **2011**, *5*, 3607–3613.

- (17) Vinogradov, N. A.; Schulte, K.; Ng, M. L.; Mikkelsen, A.; Lundgren, E.; Martensson, N.; Preobrajenski, A. B. Impact of Atomic Oxygen on the Structure of Graphene Formed on Ir (111) and Pt (111). *J. Phys. Chem. C* **2011**, *115*, 9568–9577.
- (18) Topsakal, M.; Şahin, H.; Ciraci, S. Graphene Coatings: An Efficient Protection from Oxidation. *Phys. Rev. B* **2012**, *85*, 155445.
- (19) Sen, H. S.; Sahin, H.; Peeters, F. M.; Durgun, E. Monolayers of MoS₂ as an Oxidation Protective Nanocoating Material. *J. Appl. Phys.* **2014**, *116*, 083508.
- (20) Lu, C.; Zhang, D.; van der Zande, A.; Kim, P.; Herman, I. P. Electronic Transport in Nanoparticle Monolayers Sandwiched Between Graphene Electrodes. *Nanoscale* **2014**, *6*, 14158–14162.
- (21) Peng, Z. A.; Peng, X. Formation of High-Quality CdTe, CdSe, and CdS Nanocrystals Using CdO as Precursor. *J. Am. Chem. Soc.* **2001**, *123*, 183–184.
- (22) Dean, C. R.; Young, A. F.; Meric, I.; Lee, C.; Wang, L.; Sorgenfrei, S.; Watanabe, K.; Taniguchi, T.; Kim, P.; Shepard, K. L.; et al. Boron Nitride Substrates for High-Quality Graphene Electronics. *Nat. Nanotechnol.* **2010**, *5*, 722–726.
- (23) Ferrari, A. C.; Meyer, J. C.; Scardaci, V.; Casiraghi, C.; Lazzeri, M.; Mauri, F.; Piscanec, S.; Jiang, D.; Novoselov, K. S.; Roth, S.; et al. Raman Spectrum of Graphene and Graphene Layers. *Phys. Rev. Lett.* **2006**, *97*, 187401.
- (24) Splendiani, A.; Sun, L.; Zhang, Y.; Li, T.; Kim, J.; Chim, C. Y.; Galli, G.; Wang, F. Emerging Photoluminescence in Monolayer MoS₂. *Nano Lett.* **2010**, *10*, 1271–1275.
- (25) Lee, C.; Yan, H.; Brus, L. E.; Heinz, T. F.; Hone, J.; Ryu, S. Anomalous Lattice Vibrations of Single- and Few-Layer MoS₂. *ACS Nano* **2010**, *4*, 2695–2700.
- (26) Yu, W. W.; Qu, L.; Guo, W.; Peng, X. Experimental Determination of the Extinction Coefficient of CdTe, CdSe, and CdS Nanocrystals. *Chem. Mater.* **2003**, *15*, 2854–2860.
- (27) Akey, A. J.; Lu, C.; Wu, L.; Zhu, Y.; Herman, I. P. Anomalous Photoluminescence Stokes Shift in CdSe Nanoparticle and Carbon Nanotube Hybrids. *Phys. Rev. B* **2012**, *85*, 045404.
- (28) Javier, A.; Magana, D.; Jennings, T.; Strouse, G. F. Nanosecond Exciton Recombination Dynamics in Colloidal CdSe Quantum Dots under Ambient Conditions. *Appl. Phys. Lett.* **2003**, *83*, 1423–1425.
- (29) Mak, K. F.; Sfeir, M. Y.; Wu, Y.; Lui, C. H.; Misewich, J. A.; Heinz, T. F. Measurement of the Optical Conductivity of Graphene. *Phys. Rev. Lett.* **2008**, *101*, 196405.
- (30) Mak, K. F.; Lee, C.; Hone, J.; Shan, J.; Heinz, T. F. Atomically Thin MoS₂: A New Direct-Gap Semiconductor. *Phys. Rev. Lett.* **2010**, *105*, 136805.
- (31) Deal, B. E.; Grove, A. S. General Relationship for the Thermal Oxidation of Silicon. *J. Appl. Phys.* **1965**, *36*, 3770–3778.
- (32) Wilson, L. O.; Marcus, R. B. Oxidation of Curved Silicon Surfaces. *J. Electrochem. Soc.* **1987**, *134*, 481–490.
- (33) MacCallum, J. R.; Rudkin, A. L. A Novel Technique for Measuring TH Diffusion Constant of Oxygen in Polymer Films. *Eur. Polym. J.* **1978**, *14*, 655–656.
- (34) Meek, R. L. Diffusion Coefficient for Oxygen in Vitreous SiO₂. *J. Am. Ceram. Soc.* **1973**, *56*, 341–342.